Proceedings of International Conference on Heat Exchanger Fouling and Cleaning VIII - 2009 (Peer-reviewed)
June 14-19, 2009, Schladming, Austria
Editors: H. Müller-Steinhagen, M.R. Malayeri and A.P. Watkinson

Published online
www.heatexchanger-fouling.com

CRYSTALLIZATION FOULING OF FINNED TUBES DURING POOL BOILING: EFFECT OF FIN DENSITY

M. Esawy[1], M.R. Malayeri[1] and H. Müller-Steinhagen[1,2]

1 Institute for Thermodynamics and Thermal Engineering (ITW), University of Stuttgart
Pfaffenwaldring 6, D-70550, Stuttgart, Germany, esawy@itw.uni-stuttgart.de
[2] Institute for Technical Thermodynamics, German Aerospace Centre (DLR), Pfaffenwaldring 38-40, D-70569, Stuttgart, Germany

ABSTRACT

Bubble characteristics such as density, size, frequency, and motion are key factors that contribute to the superiority of nucleate pool boiling over other modes of heat transfer. Nevertheless, if heat transfer occurs in an environment prone to fouling, the very same parameters may lead to accelerated deposit formation due to concentration effects beneath the growing bubbles. This has led to the widely accepted design recommendation to maintain the heat transfer surface temperature below the boiling point if fouling may occur, e.g. in seawater desalination. The present paper aims at investigating the formation of deposits on finned tubes during nucleate pool boiling of $CaSO_4$ solutions. The test finned tubes are low finned tubes with fin densities of 19 and 26 fins per inch made from Cu-Ni. The fouling experiments were carried out at atmospheric pressure for different heat fluxes ranging from 100 to 300 kW/m^2 and a $CaSO_4$ concentration of 1.6 g/L. For the sake of comparison, similar runs were also performed with smooth stainless steel tubes. The results show that: 1) the fouling resistance decreases with increasing fin density, 2) fouling on the finned tubes was reduced with increasing nucleate boiling activity and 3) if any fouling layer occurred on the finned tubes it could be removed easily.

1. INTRODUCTION

Nucleate pool boiling heat transfer is extensively utilized in industry as a particularly efficient mode of heat transfer. Among the widely used devices in industry in which boiling is dominant are steam generators in power plants and evaporators. If the temperature of the heat transfer surfaces is higher than the saturation temperature of the heated liquid, bubbles are generated resulting in a high degree of local turbulence and hence significantly increased heat transfer coefficients. However, if the boiling liquid contains dissolved matter, deposits start to growth beneath bubbles due to local supersaturation and steep temperature gradients (Müller-Steinhagen and Jamialahmadi, 1990). For salts with inverse solubility behaviour, concentration factors of 3-4 have been determined (Jamialahmadi et al., 1989; Jamialahmadi and Müller-Steinhagen, 1993) resulting in rapid growth and the associated drop in heat transfer coefficient and heat exchanger performance.

For heat transfer enhancement under clean conditions, numerous modified boiling surfaces have been developed and patented over the past decades. Thome (1990), Bergles (1997) and Webb (2005) have provided comprehensive reviews on the different approaches. These techniques can be categorized into two main groups of "active" and "passive" enhancements. Active techniques require external power, such as electro-magnetic fields or surface vibration. Contrariwise, passive techniques employ specific surface geometries to increase the number of nucleation sites so that the heat transfer coefficient can be increased. This then enables the enhanced surfaces to transfer the given amount of heat to a liquid with a reduced tube wall superheat. For practical reasons, passive techniques are the most viable option to enhance heat transfer during pool boiling (Ayub and Bergles, 1988; Bergles, 2002; Ayub and Bergles, 1987).

The structured surfaces are manufactured by reforming the base surface to make fins of standard or special configurations. The structured surfaces can be classified into three categories as 1) finned tubes, 2) modified finned tubes and 3) porous surface coatings. Figure 1 presents typical shapes of such structured surfaces. The first successfully used type of structured enhanced surfaces was the externally finned tube. Typical fin densities used for boiling vary from 11 to 40 fpi (fins per inch), with about 19 to 26 fpi (750 to 1026 fins per meter) being perhaps the most frequently used design (Thome, 1990). Two types of low finned tubes are depicted in Figure 1a. A modification of fin design is shown in figure 1b, where the fins are deformed mechanically to create a large number of re-entrant channels. Tubes with porous surfaces are produced by sintering or brazing small particles to the fin or smooth tube surfaces, see figure 1c.

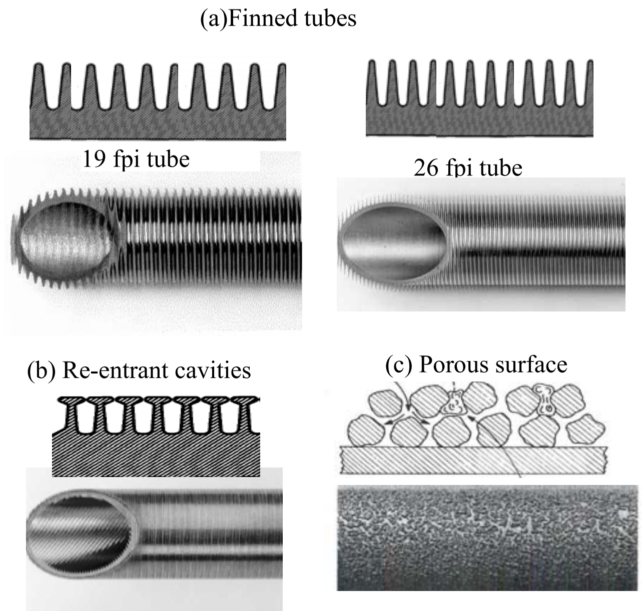

Fig. 1 Typical structures of enhanced tubes.

Although fouling is of equal concern for both plain and structured surfaces, there are only few reports in the open literatures on the investigation of fouling on structured surfaces, even for conditions where no vapour bubbles are formed. Moore (1974) demonstrated that low finned tubes tend to accumulate significantly less deposits than a smooth tube under the same operating conditions. The axial thermal expansion between adjacent fins is speculated to break the fouling layer or to keep it looser than for plain tubes. Thomas (1997) also reported that the fouling layer on low-finned tubes tends to flake-off in a plate-like form, and it was hypothesized that fins may act as knife edges for the scale formation. It was also thought that the thermal expansion and contraction of the fins during operation create a natural effect which can detach the fouling layer (Webb, 2005). Contrariwise, there have been studies which show that the impact of fins is limited to a certain range of heat fluxes (Bergles and Somerscales, 1995; Somerscales and Curcio, 1990). More notably, the previous studies are limited to a small range of heat fluxes from 20 to 80 kW/m^2 and can not be extrapolated due to strong non-linearities. The experimental results on the effect of fin density are particularly scarce.

The present study endeavors to shed some light into the fouling of low finned tubes and the effect of fin density. Systematic and carefully executed fouling runs have been carried out to discern the mechanisms of crystallization fouling during nucleate pool boiling of $CaSO_4$ solutions on finned tubes in comparison to smooth tubes under the same operating conditions. To study the effect of fin density on fouling, two types of low finned tubes with 19 and 26 fpi have been investigated. Furthermore, video recordings for clean and fouling runs were taken to interpret the experimental results.

2. EXPERIMENTAL SET-UP

2.1. Pool boiling apparatus

Figure 2 presents a schematic diagram of the pool boiling rig. With this set-up, heat transfer coefficient for various heat fluxes and $CaSO_4$ concentrations can be measured at atmospheric pressure. Its main components are boiling vessel [1], loop for steam condensation and return to the vessel, preheater [4], power control units [5], and data acquisition system to log and analyze the input and output data.

The boiling vessel [1] is a cylindrical stainless steel tank with a 304 mm inner diameter and a capacity of 30 L. Two glass view ports are provided at each end of the vessel for visual observation. The vessel is heated externally by a resistance band heater [2]. A closed flow loop including condenser [3] and preheater [4] is used to condense and preheat the evaporated liquid before returning it as saturated liquid to the vessel.

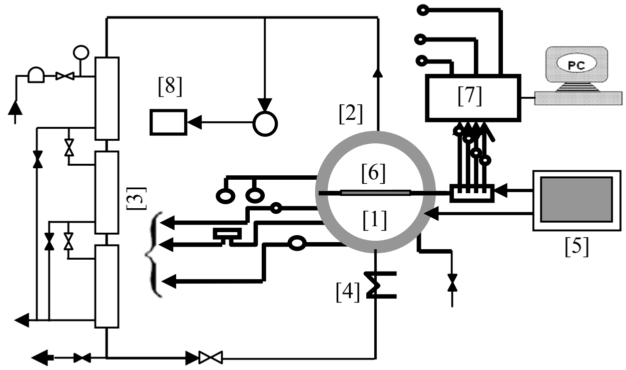

[1] Boiling vessel [2]Band heater [3] Condenser
[4] Preheater [5] Power control units
[6] Test tube [7] Data acquisition
[8] Vacuum pump

Fig. 2 Schematic diagram of the pool boiling test rig.

An electrically heated rod of HTRI design is used for the experiments. As shown in Figure 3, four E-type thermocouples are embedded into the heater to measure the wall temperature. One of these thermocouples is used to trip the power supply if the internal temperature of the heater exceeds a set limit. The condenser [3] is a three-stage single tube heat exchanger; the number of stages in operation can be adjusted according to the required heat flux. Centrally provided chilled water is used as coolant and controlled by a rotameter in conjunction with a manual flow control valve. A safety relief valve is fitted at the top of the flow circuit to relieve the pressure if it unexpectedly increases due to a failure in cooling or in power control system**.** A set of power control units [5] are utilized to adjust the input power to the heater, consisting of variable transformers with an electronic temperature controller. Boiling vessel, condenser, preheater, and all pipes are insulated to minimize the heat losses from the rig. For initial degassing of the test liquid, vacuum is drawn by a vacuum pump connected to a cold location of the condenser. To protect the vacuum pump from condensate and avoid the loss of too much vapor during degassing, a steam trap is connected with the pump.

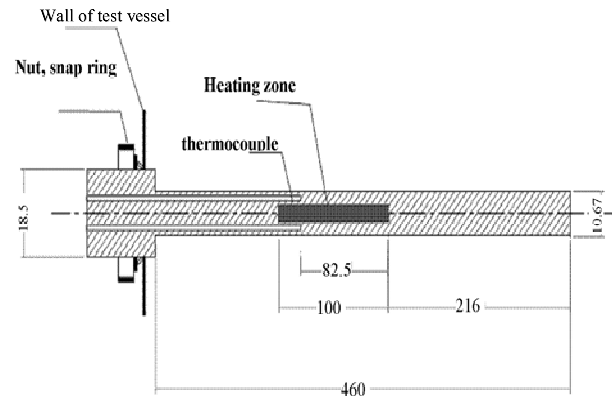

Fig. 3 HTRI cartridge heater (all dimensions in mm).

An OMEGA PXM209 absolute pressure transducer [6] is also connected to the vessel [1] to measure the pressure inside the vessel. Three K type thermocouples are inserted inside the vessel to measure the bulk temperature and the return condensate. Output from one of these thermocouples is used to trip the variac power unit if the bulk temperature exceeds a set limit.

An Agilent 34970A data acquisition system, with 34901A armature multiplexer was used for all temperature, pressure, voltage, and current measurements. A compatible PC was used to control the data acquisition unit and record all data via PCI-GPIB interface.

2.2 Test tubes

The investigated tube specimens are either smooth or finned tubes. The original stainless steel cartridge heater as shown in Figure 3 is utilized to represent the smooth tube type. The investigated finned tubes are low finned tubes with a fin density of 19 and 26 fpi (fins per inch) made from Cu-Ni alloy of CuNi10Fe1Mn type. More details of these tubes are given in Table 1 with geometrical specifications defined in Figure 4. The surface temperature of the tube can be determined by two 0.5 mm diameter K type thermocouples located at the vertically bottom and top positions of each finned tube. The holes for inserting these thermocouples into the tube wall are made by Electrostatic Discharge Machining (EDM) with 40 mm depth.

Table 1. Geometrical specifications of finned tubes.

Tube Parameter	Tube1 (19 fpi)	Tube2 (26 fpi)
Fin density (fpi)	19	26
Inner diameter(D_i), mm	10.7	10.7
Outer diameter(D_o),mm	15.7	15.7
Base diameter(D_b),mm	12.7	12.7
Fin height(h), mm	1.5	1.5
Fin pitch(m), mm	1.35	1
Wall thickness(s), mm	1	1
Tube length(L), mm	100	100
Tube surface area per length, m^2/m	0.12	0.15

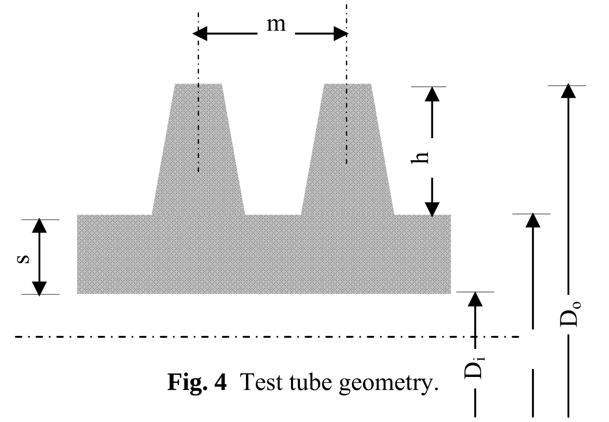

Fig. 4 Test tube geometry.

Figure 5 provides the detailed arrangement of the test tube assembly with the cartridge heater. To prepare the test tube, the fins are removed for the last 4 mm from both ends of the tube specimen, where two copper caps are soldered. The cartridge heater is then pushed tightly into the finned tube specimen, such that the heating zone of the heater is fully covered. The gap between the heater and inner tube surface is filled with a thermal conductive paste (Amazon thermal compound T12+Arctic Silver 5” with thermal conductivity of 9.8 W/m.K) to reduce the thermal contact resistance between tube and heater rod. A thermal resistive silicon paste is filled into the two cooper caps to attach the finned tube and the heater.

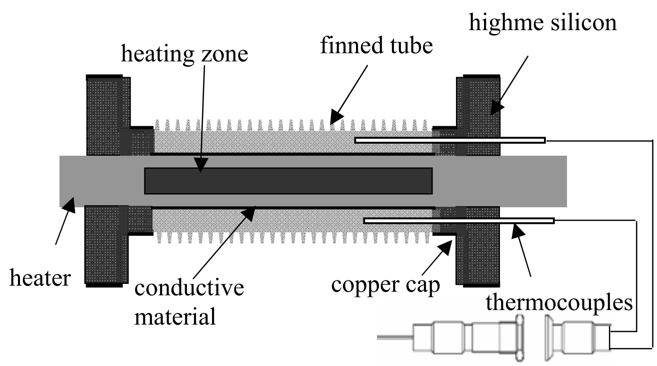

Fig. 5 Test tube assembly.

.

2.3 Preparation of $CaSO_4$ solution

Saturated calcium sulphate test solution is prepared by directly dissolving calcium sulphate hemi-hydrate ($CaSO_4$.1/2 H_2O) in distilled water. The weight of the required calcium sulphate hemi-hydrate was calculated using the following formula

$$W(\mathrm{CaSo}_4.0.5H_2O) = C_b * W(\mathrm{H}_2O) * \left(\frac{MW\ \mathrm{CaSO}_4.0.5\,\mathrm{H}_2O}{MW\ \mathrm{CaSO}_4}\right) * \left(\frac{100}{purity}\right)$$

where W is the weight and C_b is the required bulk concentration. The purity of the used calcium sulphate hemi-hydrate was found in several titration trials to be 90%. As calcium sulphate is difficult to dissolve in water, an ultrasonic device is initially used for one hour, followed by stirring at 1400 rpm for 24 hour. Then, the calcium sulphate solution was left for another day to allow any remaining particles to settle down.

2.4 Experimental procedure and data reduction

Due to the dominant influence of initial conditions on the subsequent deposition of fouling material, consistency of the experimental procedure is of prime importance. At first, the test tube has to be carefully cleaned with distilled water and finally with acetone, to remove any dust particles between the fins. The boiling vessel must also be cleaned thoroughly from any remaining deposits from the previous fouling run. Afterwards the test tube assembly will be mounted and fixed horizontally into the vessel. Before filling the vessel with solution, it should be evacuated for about one hour to check the system integrity and to remove air from the system. Prepared calcium sulphate solution will then be charged into the vessel using a 6 mm flexible sample line, until it is filled to a level approximately 3.0 cm below the top. The vessel will then be left to continue degassing until the vacuum remains constant.

Preheating of the solution to the saturation temperature was accomplished by switching on the vessel's band heater. As any dissolved gases present in the solution may affect the boiling heat transfer, a vacuum pump was used at regular intervals during preheating to remove residual gases. Simultaneously the cooling water flow to the condenser was turned on at early stages to create a natural siphon and to provide degassing of the unheated section of the test rig. The data acquisition system is switched on to assess the stability of the operating conditions. After approximately 3 hours of preheating the system becomes stable at saturation conditions.

To ensure the consistency of the results, a comparison will be made between the saturation temperature for the measured pressure and the liquid temperature measured by the thermocouples. Once steady-state conditions are confirmed, the power to the test section will be turned on by adjusting the variac power supply to the desired heat flux. The data acquisition system then records all inputs every 30 seconds and stores them as Excel spreadsheets.

For determination of heat transfer coefficients, experimental data such as bulk temperature, heat flux, and average wall temperature of the tube are required. The bulk temperature is obtained by averaging the two bulk thermocouple readings. The heat flux is calculated using:

$$\dot{q} = \frac{V.I}{A_b} \tag{1}$$

Where "V" and "I" are the measured heater voltage and current, respectively, and A_b is the base surface area of the finned tube which can be calculated as:

$$A_b = \pi . D_b . L \tag{2}$$

where D_b and L are the finned tube base diameter and tube heating zone length respectively.

The surface temperature of the tube is determined from the two thermocouples located inside the tube wall by assuming one-dimensional heat conduction through the wall as:

$$T_s = \frac{1}{2} \sum_{i=1}^{2} T_{s,i} \tag{3}$$

in which:

$$T_{s,i} = T_{th,i} - \frac{D_b . \dot{q}}{2k} \ln \left(\frac{D_b}{D_{th}} \right) \tag{4}$$

where k is the tube thermal conductivity, and D_{th} is the respective tube diameter at the position of thermocouples.

The average heat transfer coefficient can then be determined as:

$$\alpha = \frac{\dot{q}}{(T_s - T_b)} \tag{5}$$

Finally the fouling resistance due to deposition of calcium sulphate is calculated as a function of time as:

$$R_f = \left(\frac{1}{\alpha} \right)_t - \left(\frac{1}{\alpha} \right)_0 \tag{6}$$

or

$$R_f = \left(\frac{T_s - T_b}{\dot{q}} \right)_t - \left(\frac{T_s - T_b}{\dot{q}} \right)_0 \tag{7}$$

Subscripts "t" and "0" denote conditions at any time and at the beginning of the experiment when the tube is considered to be clean. This should be pointed out that boiling heat transfer coefficient at the deposit/fluid interface may change once deposits start to form on the surface due to 1) change in number of nucleation sites and 2) reduced deposit/fluid temperature (Jamialahmadi and Müller-Steinhagen, 1993)

3. RESULTS AND DISCUSSION

Calcium sulphate is an inverse solubility salt, i.e. its solubility decreases with increasing temperature. The saturation concentration of calcium sulphate at 100^{o}C is 1.6 g/L. During pool boiling, a significant increase in concentration up to 3-4 fold is expected beneath the growing bubbles (Jamialahmadi, and Müller-Steinhagen, 2004), leading to accelerated precipitation of $CaSO_4$ crystals on the surface. Fouling runs were carried out for two different finned tubes of 19- and 26-fpi made from Copper-Nickel alloy. For the sake of comparison, the original, unfinned stainless steel HTRI heater was investigated for the same operating conditions. The initial concentration of the $CaSO_4$ test solution for the fouling runs mas maintained at 1.6 g/L. The heat flux was varied between 100 and 300 kW/m^2.

3.1 Fouling of finned tubes

Figure 6 presents the variation of fouling resistance as a function of time for the 19 fpi finned tube for various heat fluxes. The shape of the finned tube's fouling curve is "asymptotic", reaching a constant value after a relatively short operating time. In this figure, the results for the heat flux of 300 kW/m^2 display an interesting trend, i.e. the asymptotic fouling resistance is lower than that for 200 kW/m^2, the opposite to what one would expect from previous work. Fouling runs for 200 and 300 kW/m^2 were repeated which the results again reaffirm the trend i.e. 300 kW/m^2 show lower fouling resistance than 200 kW/m^2 (see

Fig. 6). For smooth/plain surfaces, higher heat fluxes result in the generation of more bubbles which provide more nucleation sites for deposition (Malayeri et al, 2005). For finned tubes, however, this propensity is valid only from 100 to 200 kW/m^2 and distinguishably not from 200 to 300 kW/m^2. This maybe due to the effect of the produced bubbles which generate high shear on the fin sides as they make their way from the fin base to the bulk liquid and which depart from the fin tips with a high degree of turbulence, both being mechanisms to remove frail deposit layer from the fin and base surfaces. Visual observations clearly confirmed that the bubble detachment velocity is intensified. For a low heat flux of 100 kW/m^2, the fouling resistance fluctuates around zero indicating that only a few and scattered crystals are formed on the surface.

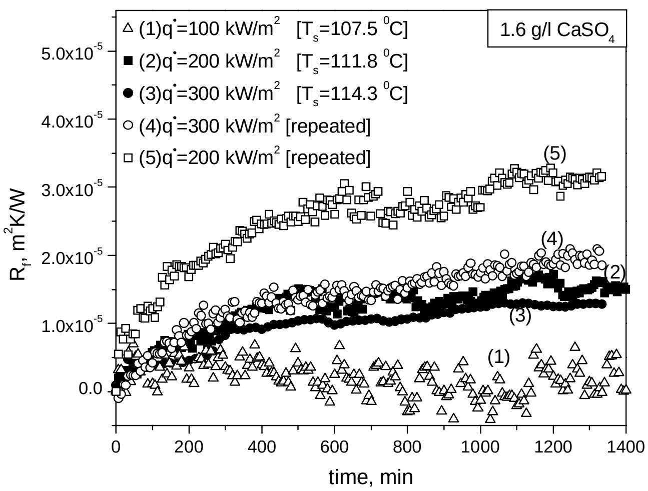

Fig. 6 Fouling resistance of the 19 fpi finned tube versus time for different heat fluxes and a $CaSO_4$ concentration of 1.6 g/L (T_s here corresponds to surface temperature at time zero).

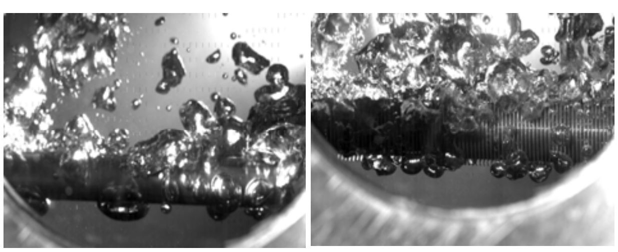

smooth tube[T_s=113 ^{o}C] finned tube[T_s=110.5 ^{o}C]

Fig. 7 Comparison of bubbles mechanisms during boiling of distilled water for the stainless steel smooth and 19 fpi tubes for a heat flux of 200 kW/m².

Fig. 7 shows two typical pictures of bubbles motion on finned and smooth tubes during boiling of distilled water for a heat flux of 200kW/m². Not surprisingly there are more bubbles on the finned tube and those bubbles that are coming from the side and bottom part of the finned tube altogether generate a higher degree of turbulence, higher than those of smooth tubes. In addition, the lower wall temperature due to the increased heat transfer from the extended surface reduces the local supersaturation and hence the fouling rate (Awad et al., 2009).

3.2 Comparisons between smooth and finned tubes

To justify the superior performance of finned tubes, it is imperative to compare their fouling trends to those of plain tubes under similar operating conditions. Figure 8 demonstrates such comparisons of the fouling resistance for the 19 fpi finned tube and a smooth tube investigated by Esawy, et al. (2009) for a heat flux of 200 kW/m^2. Note that the following resistance for the smooth tube starts at 0 m^{2}K/W as well, and increases very rapidly to the initial values shown in Fig. 8.

It is apparent that that the fouling curve for the finned tube differs from the smooth tube both quantitatively and qualitatively. The fouling resistance for the smooth tube increases rapidly until the surface of the heater reaches its maximum operating temperature of 170^{o}C after approx. 1350 minutes when the fouling run is terminated automatically. Contrariwise for the finned tube, the fouling resistance increases very slowly with time until it reaches an asymptotic value after 400 minutes. From this figure it can also be seen that the fouling resistances for the finned tube are substantially lower than those for the smooth tube. This reduction is about 90% in the given example, after 1300 min of operation.

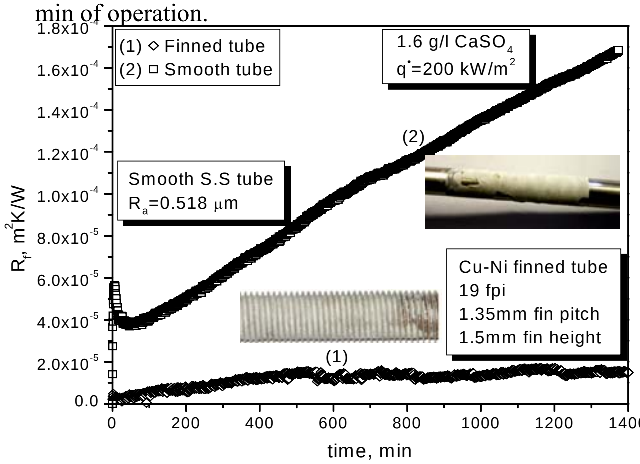

Fig. 8 Comparison of fouling resistances for smooth and finned tubes at a heat flux of 200 kW/m^2 and a $CaSO_4$ concentration of 1.6 g/l.

Pictures of the fouled tubes taken at the end of this fouling run are also shown in the same figure. The smooth tube shows a homogenous thick layer of $CaSO_4$ deposit, while the finned tube exhibits only a scattered and thin deposit layer between the fins. Post-fouling cleaning of tubes also confirmed that the deposit layer on the finned tubes could be easily washed away whereas this was not possible for the thick deposit layer on the smooth tube.

Considering the above results, the improved fouling performance of the finned tube over the smooth tube can be related to:

- The lower surface temperature provided by the extended surface of the fins. This reduces the main driving forces of crystallization fouling, namely the supersaturation of the solution.
- The wiping action of bubbles growing at the base of fins and moving along the fin surfaces. No deposits were hence found on the sides of fins above their base.
- Bubble growth and detachment behaviour on finned tubes differ substantially from plain tubes. Due to the larger number of nucleation sites, more bubbles are generated from fin areas leading to higher degree of turbulence which improves removal of the initial crystals from the surface.
- The thermal expansion and contraction of the fins during operation create a natural "self cleaning effect" which can break the fouling layer.
- The fins themselves inhibit the formation of a continuous, strongly attached fouling layer, hence promoting a scattered deposit pattern which is more susceptible to removal by shear forces.

3.3 Effect of fin density on fouling of finned tubes

As mentioned before, 19 and 26 fpi (750 and 1026 fins per meter) finned tubes are the most frequently used types in industrial boiling processes (Trewin, 1992). To study the effect of fin density under fouling conditions, it is necessary first to analyze such effects under clean boiling conditions with distilled water as working fluid.

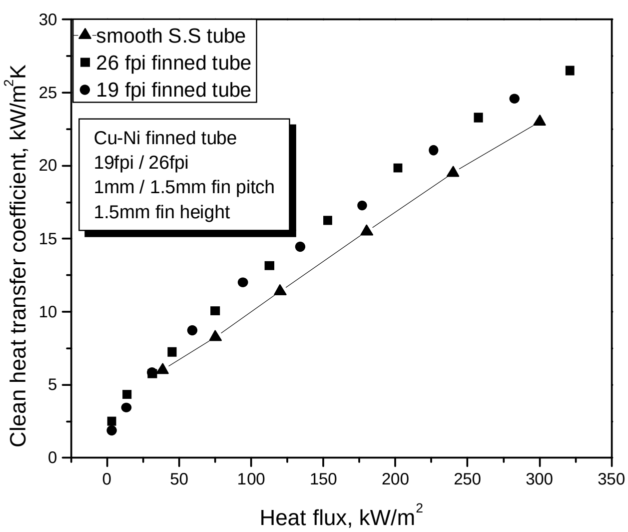

Fig. 9 Effect of fin density on clean heat transfer coefficient for 19 and 26 fpi finned tubes during boiling of distilled water.

Figure 9 depicts the clean heat transfer coefficient of distilled water versus the heat flux for both 19 and 26 fpi finned tubes as well as those of stainless steel for the sake of comparison. As can be seen, the heat transfer coefficients for the finned tube of 26 fpi are only marginally higher than those for the 19 fpi tube. This implies that fin density has only a minor impact on the thermal performance during boiling of distilled water within the range of operating conditions investigated in this study. The results are consistent with previous investigations of Ayub and Bergles (1987) and Rabas, et al. (1981).

Figure 10 shows the effect of fin density on the fouling resistance of the 19 fpi and 26 fpi tubes for a heat flux of 300 kW/m^2 and a $CaSO_4$ concentration of 1.6 g/L. This figure clearly indicates that, unlike for clean conditions, distinctively different trends exist for the two finned tubes. A reduction of 45% in fouling resistance for the 26 fpi tube over the 19 fpi tube may be observed. The figure also includes repeated results for both tubes under the same operating conditions to ensure that the trend is consistent though the reproducibility of 26 fpi is evidently better.

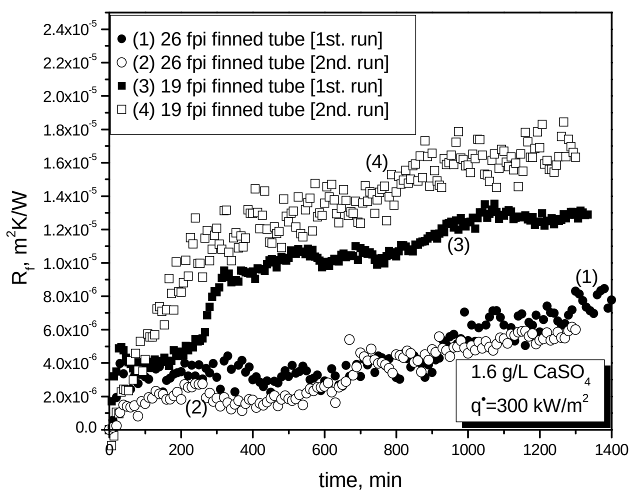

Fig. 10 Effect of fin density on fouling behavior of 19 and 26 fpi tubes for a heat flux of 300 kW/m^2 and a concentration of 1.6 g/L.

There are several reasons that may account for such different behaviour at clean and fouling conditions, i.e.:

- By decreasing the gap between the fins, the shear forces from the detaching bubbles to the fin areas will increase, enforcing the wiping action of the bubbles.
- As the fin density is increased, the remaining area at the fin base is reduced. As stated before, this is the main area where deposition was found to occur, while hardly any fouling remains attached to the fins themselves.
- By increasing the fin density, more nucleation site are available that may produce bubbles. This leads invariably to a higher degree of turbulence.
- Tentative visual observations show that the bubble detachment diameter gets smaller and the detachment velocity higher, as the fin density is increased. As a result; any scattered and fragile fouling layers between adjacent fins may be washed away more easily. However more quantitative experimental results are needed to justify these observations.

(b) 26 fpi finned tube (a)19 fpi finned tube

Fig. 11 Pictures of fouled 19 and 26 fpi finned tubes for a heat flux of 300 kW/m² and 1.6 g/l $CaSO_4$ test solution

Figure 11 shows typical pictures of the fouled 19 and 26 fpi tubes taken at the end of test runs at the same operating conditions of 300 kW/m² heat flux and 1.6 g/L The 26 fpi finned tube shows a very scattered and even thinner deposit layer than the 19 fpi tube. The observations also confirm that the deposit layer is somewhat thicker on the bottom part of the surface than the upper part. This may be due to lower surface temperature of the upper part of the tube as a result of much quicker detachment of bubbles. Post-fouling cleaning reveals that the deposit layer on both tubes can be removed easily.

Figures 12 and 13 are provided to substantiate the performance of the finned tubes over the smooth tube, as well as the effect of fin density under fouling conditions. Data included in both figures have been obtained after 1350 min of experimental time. At this time, the finned tubes have reached their asymptotic fouling resistances within the range of heat fluxes investigated in study. For the smooth tube, however, asymptotic fouling resistances have only been found for a heat flux of 100 kW/m^2; for the higher heat fluxes the fouling runs were terminated as the surface temperature exceeded its maximum set value. Fig. 12 shows the ratio of fouled to clean (at time zero) heat transfer coefficients (α_f/α_o) for the finned and the smooth tubes as a function of heat flux for a concentration of 1.6 g/L after 1350 minutes of run time. The figure shows for the smooth tube a strong reduction of heat transfer coefficient by 50% and 75% for heat fluxes of 100 and 300 kW/m^2, respectively. For the finned tubes, only 2% reduction of heat transfer coefficient occurred for the low heat flux of 100 kW/m^2. For higher heat fluxes of 200 and 300 kW/m^2, the 26 fpi tube experienced the smallest reduction of 15% and 8%, respectively, while the 19 fpi tube had a still moderate reduction of 25% and 20%, respectively.

Finally, figure 13 shows the ratio of the fouling resistance ratio of the finned tubes to that of the smooth tube after 1350 minutes of run time, as a function of heat flux for a $CaSO_4$ concentration of 1.6 g/L. From the figure, the superior performance of the 26 fpi finned tube as compared to the 19 fpi tube is evident. The best performance of finned tubes occurs at the low heat flux of 100 kW/m^2, where the fouling resistances for both finned tubes are only 1% of that of the smooth tube. The fouling resistance ratio increases as the heat flux goes up, but still reach only approximately 9%, which undoubtedly demonstrates the superiority of finned tubes over smooth tubes. Moreover, it is obvious from figures 12 and 13 that the 26 fpi finned tube exceeds the 19 fpi tube under the same operating conditions.

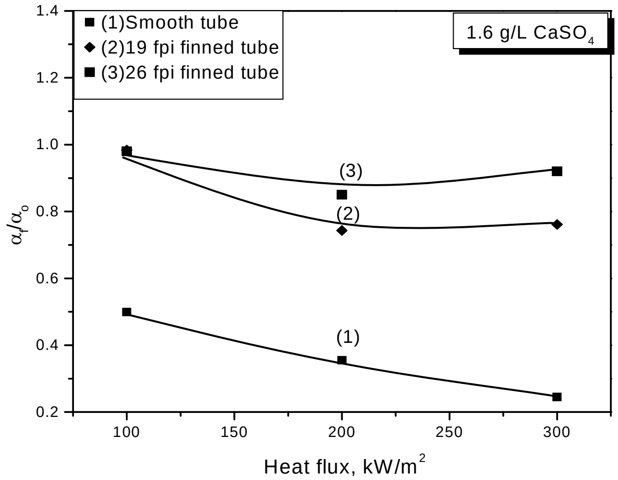

Fig. 12 Relative drop of heat transfer coefficient versus heat flux for the 19 and 26 fpi finned tubes and the smooth tube, for a concentration of 1.6 g/L $CaSO_4$

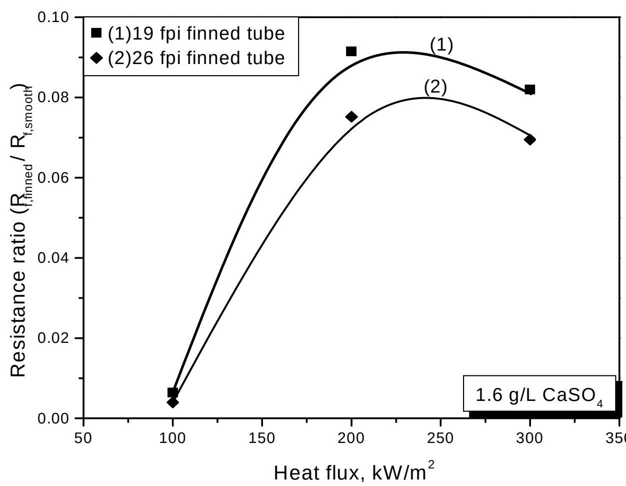

Fig. 13 Fouling resistance ratio versus heat flux for the 19 and 26 fpi finned tubes for a $CaSO_4$ concentration of 1.6 g/L.

4. CONCLUSIONS

Comparative investigation of crystallization fouling on finned and smooth tubes was performed during pool boiling of calcium sulphate. For the finned tubes, experimental results show substantial reduction of fouling compared to that for the smooth stainless steel tube used for comparison. If any deposition occurred then it was only a scattered and thin crystalline layer between the fins which could be easily removed. This differs significantly to the smooth tube which suffered from a thick and homogenous layer of deposit with strong adhesion

At high heat fluxes of 200 and 300 kW/m^2, the finned tubes still showed a significant reduction of fouling resistance of up to 95% over the smooth tube. For the heat flux of 100 kW/m^2, the fouling resistance for the finned tube fluctuated around zero. Several reasons for the superior performance of finned tubes have been provided, being related to reduced surface temperature, bubble dynamics and differential thermal expansion of fins and deposit.

Unlike its negligible effect on clean nucleate boiling heat transfer, the fin density demonstrated substantial beneficial impact on reducing fouling of the finned tubes..

NOMENCLATURE

A_b	base surface area, m^2
C_b	bulk concentration, g/L
D_b	base diameter, m
D_i	finned tube inner diameter, m
D_o	finned tube outer diameter, m
D_{th}	diameter of thermocouple location, m
h	fin height, mm
I	measured electric current
k	thermal conductivity, W/mK
L	heater heating zone length, mm
m	fin pitch, mm
MW	molecular weight, g/mol
$\dot{q}$	heat flux, W/m^2
q	heat transfer rate, W
R_f	fouling resistance, m^2K/W
T_b	bulk temperature, ^oC
T_s	surface temperature, ^oC
t	time, s
V	measured voltage, volt
W	weight, g

Greek symbol

α	heat transfer coefficient, W/m^2K

ACKNOWLEDGMENTS

The finned tubes were supplied by Wieland GmbH, Germany, for which the authors are grateful.

REFERENCES

Awad, A., Gad, H., and Yousef, A., Effect of surface temperature on particulate and crystallization fouling, IWTC, Hurghada, Egypt, pp. 1431-1442, 2009

Ayub, A.H., and Bergles, A.E., Pool boiling enhancement of a modified GEWAT surface in water, Int. J. Heat Transfer, Vol. 10, pp. 266-267, 1988.

Ayub, Z.H., and Bergles, A.E., Pool boiling from GEWA surfaces in water and R-113, J. Wärme- und Stoffübertragung, Vol. 21, pp. 209-219, 1987.

Bergles, A.E., and Somerscales, E.F.C., The effect of fouling on enhanced heat transfer equipment, J. Enhanced Heat Transfer, Vol. 2, pp. 157-166, 1995.

Bergles, A.E., Enhancement of pool boiling, Int. J. Refrigeration, Vol. 20, pp.545-551, 1997.

Bergles, A.E., ExHFT for fourth generation heat transfer technology, J. Experimental Thermal Fluid Science, Vol. 26, pp. 335-344, 2002.

Bornhorst, A., Zhao, Q. and Müller-Steinhagen, H., Reduction of scale formation by ion implantation and magnetron sputtering on heat transfer surfaces, J. Heat Transfer Eng., Vol. 20, part 2, pp. 6-14, 1999.

Esawy, M., Malayeri, M.R. and Müller-Steinhagen, H., Mechanism of crystallization fouling during pool boiling of finned tubes, IWTC, Hurghada, Egypt, pp. 1417-1430, 2009

Jamialahmadi, M., and Müller-Steinhagen, H., A new model for the effect of calcium sulfate scale formation on pool boiling heat transfer, ASME, J. Heat Transfer, Vol.126, pp. 507-517, 2004.

Jamialahmadi, M., and Müller-Steinhagen, H., Scale formation during nucleate boiling - A review, Corrosion Reviews, Vol. 11, Part 1&2, pp. 25-54, 1993.

Jamialahmadi, M., Blöchl, R., and Müller-Steinhagen, H., Bubble dynamics and scale formation during nucleate boiling of aqueous calcium sulphate solutions, Chemical Engineering and Processing, Vol. 26, pp. 15-26, 1989.

Malayeri, M.R., Müller-Steinhagen, H. and Bartlett, T.H., Fouling of tube bundles under pool boiling conditions, J. Chem. Eng. Sci., Vol. 60, part 6, pp. 1503-1513, 2005.

Moore, J., Fin tubes foil fouling for scaling services, Chemical Processing, Vol. 37 No. 8, pp. 8-10, 1974.

Müller-Steinhagen, H. and Jamialahmadi, M., Scale formation during boiling - the effect of heat flux and $CaSO_4$ concentration, ASME, paper no. 90-WA/HT-3, 1990.

Rabas, T. J., Eckels, P. W., and Sabatino, R. A., The effect of fin density on the heat transfer and pressure drop performance of low finned tube banks, Chemical Eng. Comm., Vol. 10, No. 1-3, pp. 127-147, 1981

Somerscales, E.F.C., and Curcio, L.A, Effect of calcium sulphate on pool boiling of enhanced surfaces, ASME WAM, Dallas, Texas, 1990.

Trewin, R. R., Enhanced boiling heat transfer in horizontal tube bundles, Heat Transfer Laboratory Report, No.HTL-13, 1992

Thomas, C., Recent developments in the manufacturing and application of integral low fin tubing in titanium and zirconium, in Zirconium/Organics Conference, Gleneden Beach, Oregon, Proceedings, pp. 169, 1997.

Thome, J.R., Enhanced boiling heat transfer, Hemisphere Publishing Corp., New York, pp. 40, 1990.

Webb, R.L., Principles of enhanced heat transfer, John Wiley and Sons, Inc., pp. 3-10, 2005.